Radio Science, Volume 36, Number 3, Pages 483–498, May/June 2001

Tracking tropospheric radio occultation signals from low Earth orbit

Sergey V. Sokolovskiy[1]
GPS Science and Technology Program, University Corporation for Atmospheric Research, Boulder, Colorado

Abstract. Propagation of radio occultation signals through the tropical lower troposphere with severe refractivity gradients results in significant spreading of the signal spectrum. Under such conditions a signal acquisition technique which tracks large random troposphere-induced phase accelerations more reliably than a generic phase-locked loop has to be applied. This paper discusses the results of simulations of open loop tracking of radio occultation signals that were generated with data from high-resolution tropical radiosondes. The signal has to be down-converted in real time in the receiver on orbit to a low mean residual frequency by use of a phase (Doppler) model based on predicted orbits and refractivity climatology. The down-converted complex signal is then low-pass filtered and sampled. The phase in excess of the phase model must be reconstructed from the sampled and down-linked signal in postprocessing. This may require an additional down-conversion to eliminate (minimize) aliasing of harmonics in the spectrum. Then the accumulated phase can be reconstructed by resampling the signal at a higher rate to resolve the cycle ambiguities. A fast algorithm for prediction of the Doppler based on the refractivity climatology and an algorithm for the detection of Doppler mismodeling based on sliding window spectral analysis of the down-converted signal are developed and tested. The accuracy of the Doppler modeling, ±(15-20) Hz, the required filter bandwidth, 100 Hz, and the sampling rate, 50-100 Hz, are estimated.

1. Introduction

A typical Global Positioning System (GPS) receiver provides phase and amplitude of a signal as output of a digital phase-locked loop (PLL) [*Stephens and Thomas,* 1995; *Kaplan,* 1996]. Such a receiver was used for tracking of the radio occultation (RO) signals in the GPS/Meteorology (GPS/MET) experiment [*Kursinski et al.,* 1997; *Rocken, et al.,* 1997; *Schreiner et al.,* 1998]. However, the dynamics of the RO signals propagated through the lower troposphere and received by a low Earth orbit (LEO) satellite are rather complicated [*Sokolovskiy,* this issue]. Random phase accelerations of the signal can be significantly larger than allowed for stable operation of the PLL in a generic GPS receiver [*Kaplan,* 1996]. It is not clear whether PLL, which is an optimal tracking technique for single-tone signals with noise, is adequate for tracking multitone RO signals and preserving all necessary information content. Also, PLL tracking will result in loss of some amount of the lower tropospheric data, especially for rising occultations. Thus a different signal acquisition technique in the lower troposphere has to be applied in the future RO missions [*Kuo et al.,* 2000]. An alternative technique is open loop (OL) tracking, which had been applied in planetary occultation studies [*Lindal et al.,* 1983, 1987]. OL tracking is basically raw sampling of the complex signal, and it allows tracking of both setting and rising occultations. However, wideband sampling as applied in the planetary occultation studies would result in downlinking of a large amount of data from LEO, which

[1]Also at A. M. Obukhov Institute of Atmospheric Physics, Moscow, Russia.

Paper number 1999RS002305.
0048-6604/01/1999RS002305$11.00

is expensive and not needed to preserve the information content of that data. A generic implementation of the OL tracking technique for Earth's troposphere must include in-real-time down-conversion of the signal with the use of a predicted phase (Doppler) model, low-pass filtering, and sampling of the complex signal. Then the phase in excess of the phase model must be reconstructed from the sampled complex signal in postprocessing. An important difference betwen OL and PLL tracking is that in OL there is no feedback between the received signal and the phase model which is thus under control. In PLL the phase model is recurrently updated in real time on the basis of projection ahead (extrapolation) of the previously extracted phase and may be subjected to an uncontrolled deviation from the true phase of the signal when complicated signal dynamics are tracked [*Stephens and Thomas,* 1995], thus resulting in corruption of the output signal. It is believed that this was the primary reason for the large refractivity retrieval errors including bias observed during the GPS/MET experiment in the lower troposphere [*Rocken et al.,* 1997].

In this paper we use the RO signals that are simulated based on high-resolution tropical radiosondes with a diffractional (multiple phase screens) technique [*Sokolovskiy,* this issue] for the L1 GPS frequency of 1.57542 GHz. The selected radiosondes captured very complicated vertical moisture structures in the tropical troposphere. These structures result in severe refractivity gradients in the tropical lower troposphere and in large phase and amplitude fluctuation of RO signals. The modeling assumes a descent (ascent) rate of the line of sight (the straight line transmitter-receiver) of 3.2 km s^{-1}, which is about the maximal possible rate corresponding to GPS and LEO (750 km altitude) moving in coplanar orbits in opposite directions. Thus the random phase acceleration and the spectral bandwidth of the simulated RO signals introduce "worst case" conditions. An example of such a signal is shown in Figure 1 (based on the radiosonde launched at 7.1° N, 171.4° E, October 19, 1995, 1200 UTC). Figures 1a and 1b show amplitude and excess Doppler frequency shift of the signal (i.e., in excess of the Doppler shift in vacuum) sampled at 50 Hz rate. The horizontal scale shows the time and the altitude of the line of sight related by a factor of 3.2 km s^{-1}. As seen from Figures 1a and 1b, the structure of the RO signal is substantially changed after ~10 s, that is, after the signal descends into the moist troposphere. Figures 1c, 1d, and 1e show the spectra (modulo the spectral amplitude) of the complex RO signal calculated within 2.56 s windows (after removal the second-order least squares fit from the phase). As seen from Figures 1c, 1d, and 1e the double-sided spectral bandwidth of the RO signal is ~10 Hz above the moist troposphere and ~50 Hz below. At low line of sight altitudes the shape of the spectrum is asymmetric (discussed by *Sokolovskiy* [this issue]).

We simulated closed-loop tracking of the modeled RO signals. For this simulation we recurrently extracted the residual phase after down-conversion with a phase model obtained from extrapolation of the previously extracted phase. This simple tracking shows very stable results above the moist troposphere. However, in the moist troposphere the modeled tracking is unstable. In particular, the result substantially depends on the amount of the previously extracted data used for the extrapolation of phase and on the method of extrapolation. It was not possible to tune up the algorithm to obtain stable results for all modeled data, and sometimes the tracking errors were very large. The sensitivity of PLL tracking to tunable parameters was also observed in the GPS/MET results. The minimal altitude of the line of sight (below which the GPS/MET receiver was losing lock) and the magnitude of the refractivity bias were substantially different between one observational period, June-July 1995, and all other observational periods. For the June-July 1995 period the receiver tracking firmware had been modified by the Jet Propulsion Laboratory [*Kuo et al.,* 2000]. Figure 2 shows the minimal altitude of the line of sight as a function of latitude for all occultations observed during the June-July 1995 and October 1995 periods. For the June-July 1995 period the RO signals were tracked substantially lower. Another important difference can be seen in Figure 2. Typically (like in October 1995), the receiver loses lock in the tropics at greater heights than away from the equator. This is attributed to the strong fluctuation of the RO signals in the tropics and can clearly be seen in the right graph of Figure 2. However, for the June-July 1995 period the situation is opposite. This can be explained by propagation of radio waves down to lower line-of-sight altitudes due to diffraction by the laminated structure of the refractivity in the moist tropical troposphere [*Sokolovskiy,* this issue]. If we assume that the modification of the tracking technique for the June-July 1995 period made it less susceptible to losing lock due to signal fluctuation, then,

in fact, the RO signals can be tracked down to lower altitudes in the tropics because of the larger mean signal power.

This paper considers an implementation of the OL technique for tracking L1 GPS RO signals that passed through the Earth's lower troposphere and are received in LEO. This technique is validated by numerical simulations using modeled RO signals.

Section 2 introduces an algorithm for the prediction of the mean Doppler frequency shift of RO signals based on predicted GPS and LEO orbits and on a model of the signal bending angles. The model of the bending angles is calculated in advance by ray tracing using the refractivity profiles given by a climatological model. Since the ray tracing can be carried out in advance, the algorithm for the prediction of the Doppler is computationally fast and can operate in the receiver on board LEO. This algorithm is applied to a large ensemble of the refractivity profiles from the National Centers for Environmental Prediction (NCEP) T62 numerical weather prediction (NWP) model. The Doppler differences for given GPS and LEO orbits provide an estimate of the potential accuracy of the Doppler prediction with the use of climatology. The Doppler predicted with the use of climatology is compared to the Doppler modeled from high-resolution radiosondes and to the GPS/MET observational Doppler. The latter comparison clearly reveals tracking errors of the GPS/MET receiver.

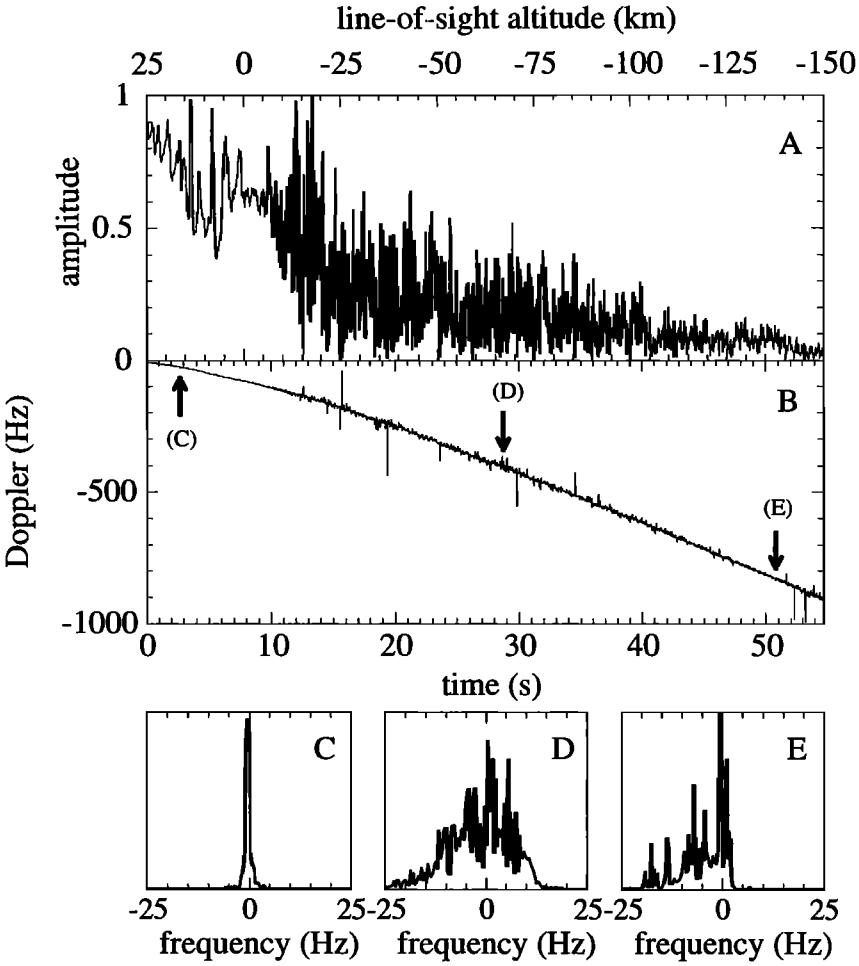

Figure 1. A model of the tropospheric RO signal: (a and b) amplitude and excess Doppler sampled at 50 Hz rate and (c-e) spectra of the signal at altitudes indicated by arrows in Figure 1b.

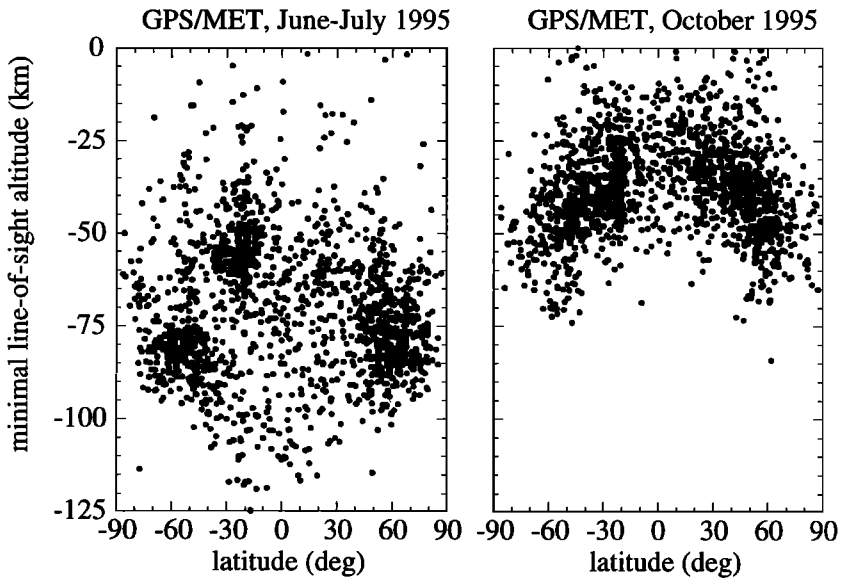

Figure 2. Minimal altitude of the line of sight (straight line GPS-LEO) for all GPS/MET occultations during two observational periods.

In section 3 the OL tracking of a RO signal which includes down-conversion, low-pass filtering, and sampling is outlined. The required filtering and sampling bandwidths are evaluated.

Section 4 discusses postprocessing of the complex sampled RO signal which includes reconstruction of the amplitude and the continuous (accumulated) phase. For the signals sampled with aliasing (but without overlapping of harmonics) an algorithm is introduced which allows us to estimate the mean Doppler mismodeling by detecting the shift of the center in the sliding spectrogram. This shift as a function of time is used as the frequency model for an additional down-conversion of the RO signal (which eliminates or substantially reduces the aliasing in the spectrum) prior to the reconstruction of phase and amplitude. The effect of thermal noise on the reconstructed phase is also evaluated.

In section 5 the "tracked" RO signal is subjected to radio holographic inversion. This allows us to demonstrate the effects of "tracking errors" and of thermal noise on the reconstructed refractivity.

In this paper the transmitted signals are assumed to be monochromatic. Demodulation of the GPS signals (i.e., removal of pseudorandom and data phase modulations) is not considered. The principles of in-real-time demodulation by means of delay-locked loop are given by *Kaplan* [1996]. In particular, the problem of the estimation of the antenna gain required for reliable demodulation under conditions of low signal power should be addressed in a separate study. Since the ionospheric correction is not so important for tropospheric profiling by the occultation technique, it is sufficient to track only the L1 C/A signal in OL mode.

2. Prediction of the Doppler Frequency Shift of the RO Signal

In this section we introduce an algorithm for predicting the Doppler frequency shift of the RO signal with the use of a refractivity climatology and discuss the accuracy of this prediction. We assume that GPS and LEO orbits can be predicted accurately enough just prior to an occultation. Given the orbits and some model of the atmospheric refractive index $n(z, \theta)$, where z is altitude over the reference ellipsoid and θ is latitude, the Doppler may be predicted by means of ray tracing. However, this is not efficient, meaning that the prediction has to be computed prior to each occultation in the receiver operating in LEO. It is more efficient to calculate in advance the bending angle α as a function of the height of the ray asymptote h and of the latitude of the ray tangent point θ under the assumption of local spherical symmetry of refractivity

$$\alpha(h,\theta) = -2a\int_a^\infty \frac{\partial[\ln n(z,\theta)]/\partial z}{\{[r_c(\theta)+z]^2 n^2(z,\theta) - a^2\}^{1/2}} dz, \quad (1)$$

where $a = r_c(\theta)+h$ is the impact parameter and $r_c(\theta)$ is the local curvature radius of the Earth's reference ellipsoid. The function $\alpha(h,\theta)$ is defined for $h(\theta) > h_{\min}(\theta) = r_c(\theta)[n(0,\theta)-1]$ ($h_{\min}$ corresponds to the ray touching the reference ellipsoid). The function $\alpha(h,\theta)$ does not depend on orbits. It must be parameterized and uploaded to the receiver. Prediction of the Doppler is then done in two steps: (1) calculation of the angles ϕ_1, ϕ_2 between ray tangent and local vertical at the transmitter and receiver (i.e., ray zenith angles) for given radius vectors of the transmitter and receiver $\mathbf{r}_1$, $\mathbf{r}_2$ (in the reference frame centered at the local center of curvature of the reference ellipsoid under the estimated ray tangent point) and (2) calculation of the Doppler frequency shift for the given zenith angles ϕ_1, ϕ_2 and radius vectors and velocities of the transmitter and receiver $\mathbf{r}_1$, $\mathbf{r}_2$, $\mathbf{v}_1$, $\mathbf{v}_2$.

Ray zenith angles ϕ_1 and ϕ_2 can be calculated by concurrent solving of the following equations

$$r_1 \sin\phi_1 = r_c(\theta) + h \quad (2a)$$

$$r_2 \sin\phi_2 = r_c(\theta) + h \quad (2b)$$

$$\phi_1 + \phi_2 + \beta - \alpha(h,\theta) - \pi = 0, \quad (2c)$$

where β is the central angle between $\mathbf{r}_1$ and $\mathbf{r}_2$. Equations (2a) and (2b) introduce Snell's law. Equation (2c) is just the identity which follows from the definition of all included terms. Given a first guess of the latitude of ray tangent point θ (say, assuming a straight line between $\mathbf{r}_1$ and $\mathbf{r}_2$, or using already estimated θ for the previous positions of the satellites) the equations (2a)-(2c) are solved for h, ϕ_1, and ϕ_2 with the use of an iterative method (until the increment in h is smaller than some prespecified value). Then the direction vector to ray tangent point is calculated by rotating vector $\mathbf{r}_1$ toward $\mathbf{r}_2$ around the normal to the occultation plane by the angle $\pi/2 - \phi_1 + \alpha/2$, and this allows one to adjust θ. Then the solution of (2a)-(2c) is repeated with the adjusted θ (until the increment in θ is smaller than some prespecified value).

As was shown by *Sokolovskiy* [this issue] diffraction by the small-scale laminated structures of refractivity in the moist troposphere results in propagation of RO signals down to very low line-of-sight altitudes. It may happen that for the refractivity model which is used to calculate $\alpha(h,\theta)$ there is no ray connecting the transmitter and receiver for large enough values of the central angle β. However, since the diffracted RO signal exists for those β and its information content is important for radio holographic inversions, the signal must be tracked and the Doppler has to be predicted. For those β where (2a)-(2c) have no solution (i.e., $h < h_{\min}$) we assume that the ray is "sliding" along the Earth's surface, thus accumulating the additional bending complementary to $\alpha(h_{\min},\theta)$, while the height of the ray asymptote remains constant, $h = h_{\min}$. In this case, $\phi_1 = \phi_{1\,\min}$, and $\phi_2 = \phi_{2\,\min}$ are constants which are calculated from (2a) and (2b) for $h = h_{\min}$. Then the total bending angle (which is necessary for the adjustment of θ) is calculated from (1c), $\alpha = \phi_{1\,\min} + \phi_{2\,\min} + \beta - \pi > \alpha(h_{\min},\theta)$.

The discussed calculation of ϕ_1 and ϕ_2 with the use of two nested loops is computationally inexpensive since (2a)-(2c) are simple algebraic equations (the most computational expense is in the calculation of $\alpha(h,\theta)$ by means of (1), but this has to be done in advance). The parameterized function $\alpha(h,\theta)$ can be periodically uploaded to the receiver to trace the seasonal variability in climatology. However, it is also possible to use some standard model $\alpha(h)$ for all latitudes and seasons at the expense of some insignificant reduction in accuracy of the Doppler model (the accuracy is discussed below).

Once the ray zenith angles ϕ_1 nd ϕ_2 have been computed, the model of the Doppler frequency shift of the RO signal f_{dop} can be calculated by using the equation [*Kursinski et al.*, 1997]

$$f_{\text{dop}} = fc^{-1}[\pm v_{\text{op1}}\cos(\gamma_1 - \phi_1) \pm v_{\text{op2}}\cos(\gamma_2 - \phi_2)], \quad (3)$$

where c is the light velocity in the vacuum, f is the carrier frequency, $\mathbf{v}_{\text{op1,2}}$ are the projections of the velocity vectors of transmitter and receiver on the occultation plain, and $\gamma_{1,2}$ are the angles between those projections and local verticals at the transmitter and receiver (plus or minus depends on the directions of the vectors $\mathbf{v}_{\text{op1,2}}$). The accuracy of (3), which is the first order expansion in v/c of the exact relativistic equation for the Doppler [*Vorob'ev and Krasil'nikova*, 1994], is better than 1 Hz.

To estimate the possible accuracy of the Doppler prediction, the following numerical modeling was performed. The satellite orbits were fixed circular and coplanar, r_1 =26,600 km, r_2 =7150 km, v_1 =3.9 km s^{-1}, v_2 =7.5 km s^{-1} (the satellites move in op-

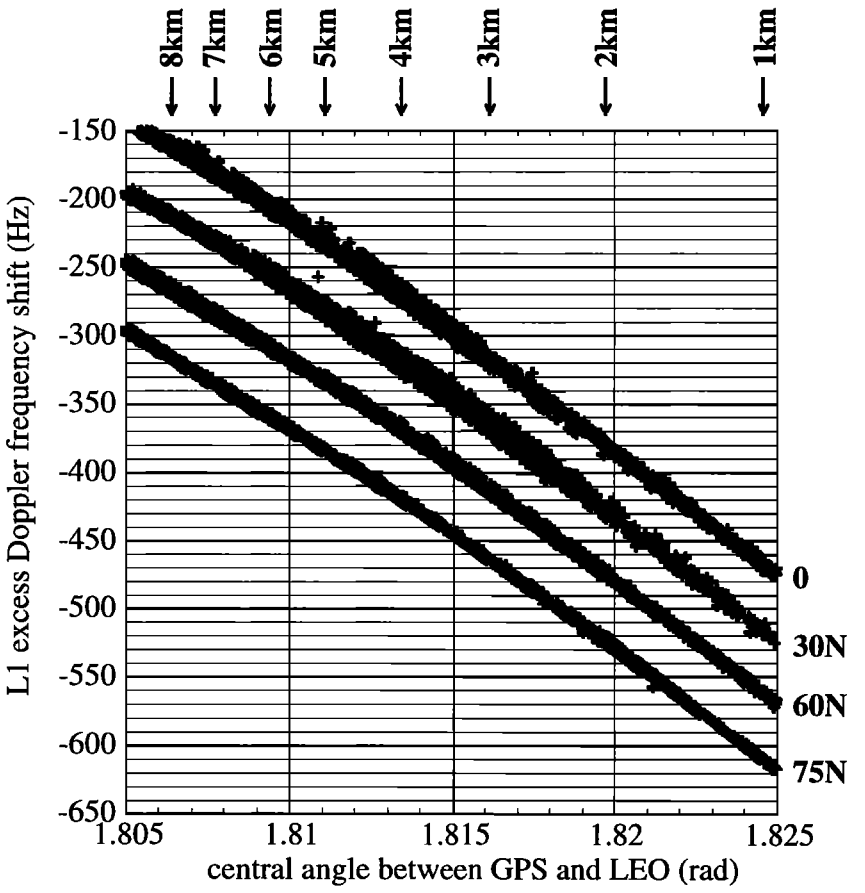

Figure 3. The spread of the mean Doppler frequency shift of RO signals estimated with the use of NCEP T62 NWP model. Different ensembles (each of 192 profiles) correspond to different latitudes (indicated at the right). The ensembles are shifted in frequency domain by 0, -50, -100, and -150 Hz for display purposes. The arrorws with the numbers (on top) indicate approximate altitudes of ray tangent point.

posite directions), and r_c =6370 km. The Doppler function $f_{\rm dop}(\beta)$ was obtained by solving (2a)-(2c) and (3) when the bending angle profiles $\alpha(h)$ were calculated for a large ensemble of vertical refractivity profiles reproduced by the NCEP T62 NWP model [*Sela*, 1980]. This model has a horizontal resolution of ~1.9° in latitude and longitude, and 28 levels in altitude, providing a vertical resolution of ~0.1 km near the Earth's surface, and several kilometers near the top (at ~30 km altitude). Figure 3 shows four ensembles of the excess Doppler $\Delta f_{\rm dop}(\beta) = f_{\rm dop}(\beta) - f^0_{\rm dop}(\beta)$, where $f^0_{\rm dop}(\beta)$ is the Doppler shift due to the motion of the satellites in space (i.e., calculated for $\alpha(h) = 0$). Each ensemble consists of 192 profiles calculated for a given latitude (indicated in the figure) and for different weather conditions at that latitude (ensembles for different latitudes are shifted in frequency for display purposes). Approximate altitudes of ray tangent points are indicated by arrows on top. The "spread" of each ensemble gives an estimate of how well mean (smoothed) Doppler could be predicted with the use of the climatology for that latitude. The largest spread, of about ±15 Hz, is in the tropics, at ray tangent point altitudes of ~3-5 km. Thus the mean Doppler frequency shift during an occultation can be predicted with an accuracy of about ±15 Hz with the use of climatology which depends on latitude and sea-

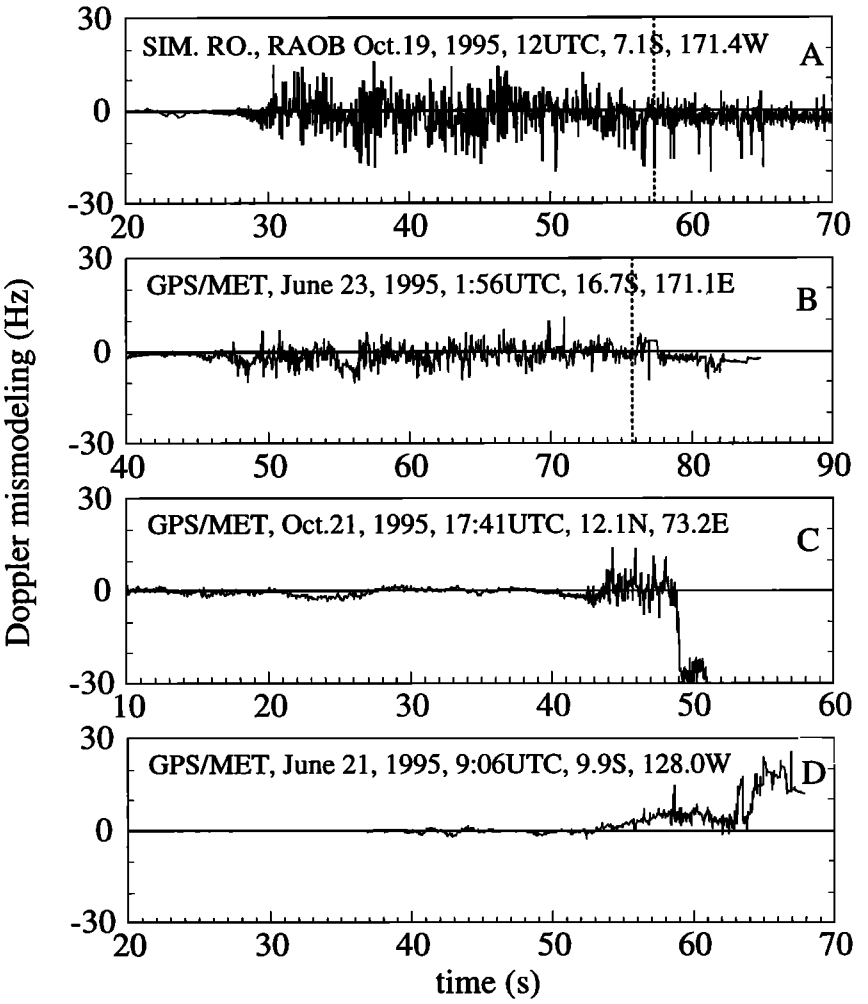

Figure 4. The difference between the true Doppler of the RO signal and the Doppler model (predicted based on satellite orbits and refractivity climatology): (a) RO signal simulated from high-resolution radiosonde and (b-d) GPS/MET RO signals.

son. If to use all-latitude and all-season climatology the mean Doppler can be predicted with an accuracy of about ±15-20 Hz.

The small weather-related spread of the mean Doppler frequency shift of a RO signal, which allows its prediction (modeling) with the use of climatology with an accuracy of ~15-20 Hz (the excess Doppler by itself may be of the order of ~1 kHz) has a clear explanation. This spread is related to the spread of arrival angles of rays received in LEO, and thus it depends on the distance from the receiver to the limb. The larger this distance is, the smaller is the angular size of the atmosphere as viewed from the receiver, and thus the smaller is the spread of arrival angles (for given atmospheric properties). For the distance of 3000 km the spread of arrival angles (which corresponds to the spread of altitudes of ray tangent point around some mean) is ~10 times smaller than the spread of bending angle for that mean altitude of ray tangent point. While the spread of the frequency of the RO signal decreases with increasing distance between the receiver and Earth's limb, the duration of the signal increases.

The ionosphere causes an additional Doppler shift of the order of ~1-2 Hz when the ray tangent point is at tropospheric altitudes. In principle this shift can

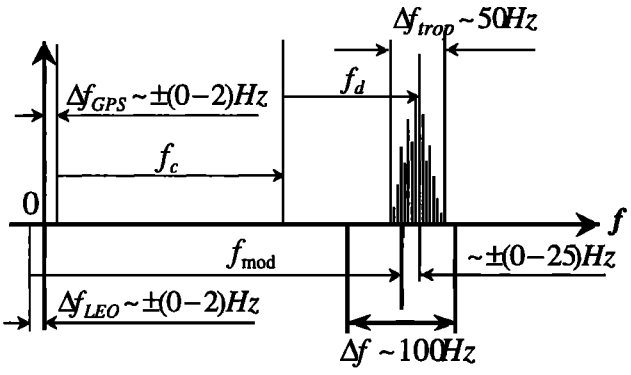

Figure 5. Layout of the RO signal and its model in the frequency domain.

be modeled with the use of some ionospheric climatology, but the ionosphere is much more changeable than the neutral atmosphere. Since the ionospheric Doppler is much smaller than the spread of the neutral atmospheric Doppler, for the OL tracking the ionospheric Doppler can be neglected.

For validation of the introduced algorithm we used the refractivity calculated from the CIRA+Q model [*Kirchengast et al.*, 1999]. This model is based on pressure and temperature from CIRA86, but it additionally includes the partial pressure of water vapor below 15 km. On the basis of this climatology we "predicted" the Doppler for the RO signal shown in Figure 1. The difference between the "true" and predicted Doppler (i.e., the Doppler mismodeling) is shown in Figure 4a. As seen, the maximal mean Doppler mismodeling is within ±10 Hz. To the right of the vertical dashed line, the CIRA+Q refractivity does not allow rays to connect the transmitter and receiver, and the Doppler was predicted with the use of rays "sliding" along the Earth's surface as discussed earlier in this section. Next, we "predicted" the Doppler for GPS/MET occultations by using positions and velocities of the GPS and LEO and CIRA+Q for the month when the occultation was observed. We used only the occultations which reached an excess phase larger than 1 km. Some examples are shown in Figures 4b-4d. Figure 4b shows the Doppler mismodeling for the occultation with the lowest penetration during the June-July 1995 observational period (-125 km of the line-of-sight altitude, as can be seen in the left graph of Figure 2). Again the mean Doppler mismodeling is within ±10 Hz. After ~76 s one can see several sections of the signal with significantly reduced fluctuation of Doppler, which cannot be explained by propagation in the troposphere (compare to Figure 4a which shows homogeneous structure of the fluctuation). We believe that these sections are indicative of GPS/MET receiver tracking errors. Other examples of the tracking errors are shown in Figures 4c and 4d. Figure 4c shows the 25 Hz Doppler offset at the end of tracking, which is a rather common tracking error for the GPS/MET receiver whose digital PLL operates at a 50 Hz rate. However, this error can be detected and the corrupted data truncated (or corrected). Figure 4d shows a tracking error that is more difficult to detect. The structure of the Doppler changes after ~63 s and it clearly differs from what we consider a normal tropospheric signal. It includes a positive bias in Doppler (for setting occultations this corresponds to a negative bias in accumulated phase). We believe that RO signals like the one shown in Figure 4d can be responsible for the significant portion of the negative refractivity bias in the troposphere reported for the GPS/MET experiment [*Rocken et al.*, 1997]. In most cases (but not always) these GPS/MET receiver tracking errors occur under conditions of low signal-to-noise Ratio (SNR), and this can be used for truncation of the RO signals. For OL tracking with the use of a predicted Doppler model, low SNR and even temporary disappearance of the signal do not introduce a problem.

3. Open Loop Tracking of RO Signal

A schematic layout of the received and modeled RO signals in the frequency domain is shown in Figure 5. In addition to the carrier frequency transmitted by GPS, f_c, there is a Doppler shift f_d (which includes the relativistic effects), and finally, the spectrum of the signal is spread by $\Delta f_{\text{trop}} \lesssim$ 50 Hz because of diffraction by the small-scale laminated structure of refractivity in the troposphere. Besides the special shift to account for the main portion of the relativistic effects in Doppler (-0.7 Hz for the L1 signal), the GPS transmitted frequency f_c may have an artificially introduced uncertainty $\Delta f_{\text{GPS}} \lesssim 2$ Hz (selective availability, S/A; *Rocken and Meertens* [1991]; even though at present S/A is cancelled, it can still be taken into account). The signal must be down-converted in the receiver with the use of the frequency model, $f_{\text{mod}} = f + f_{\text{dop}}$, based on predicted GPS and LEO orbits and refractivity climatology, as discussed in section 2 (equation (3)). An additional error in the frequency model

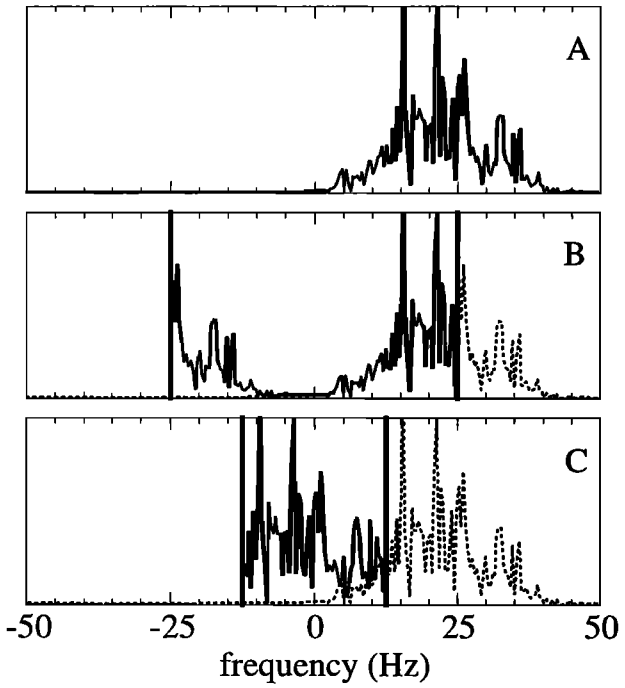

Figure 6. Spectra of the RO signal (dashed lines) after sampling at different rates (solid lines): (a) 100 Hz, no aliasing; (b) 50 Hz, aliasing without overlapping of harmonics; (c) 25 Hz, aliasing with overlapping of harmonics.

f_{mod} is introduced by the receiver clock when modeling the GPS carrier frequency f. This error, Δf_{LEO}, which depends on the receiver clock stability, is estimated as $\lesssim 2$ Hz for the GPS/MET receiver (W.S. Schreiner, personal communication, 2000), and it can be reduced in the future receivers by using more stable oscillators. Thus after the down-conversion the mean frequency of the RO signal is shifted from zero because of neutral atmospheric mismodeling (~15-20 Hz), ionospheric mismodeling (~1-2 Hz), receiver clock error (~0-2 Hz), possible S/A transmitter (GPS) clock error (~0-2 Hz), and relativistic effects not modeled by the special GPS carrier frequency shift (<1 Hz). Thus the maximal mean frequency mismodeling of RO signal can be estimated as ~25 Hz. The estimate of the maximal single-sided troposphere-induced spread of the RO signal spectrum is ~25 Hz [*Sokolovskiy,* this issue]. Thus the down-converted RO signal may occupy at maximum ±50 Hz frequency domain. To minimize noise aliasing, it must be at first low-pass filtered with 100 Hz bandwidth, then sampled in phase and quadrature and down-linked to the ground. The sampling rate generally has to be equal to the spectral bandwidth of the signal, that is, 100 Hz. However, since the spread part of the spectrum (where the main signal power is concentrated) occupies only part of the full spectral band, the sampling rate may be lower. This is discussed in section 4.

4. Postprocessing of the Complex Sampled RO Signal

Figure 6 shows the spectrum of the down-converted RO signal sampled at different rates. When the sampling rate is greater or equal to the full spectral bandwidth of the signal, that is, ~100 Hz, the spectrum is reproduced without aliasing and the signal may be completely recovered from its complex samples (as follows from the sampling theorem [e.g., *Proakis and Manolakis,* 1992]). This situation is shown in Figure 6a (100 Hz sampling rate). Lower sampling rates may result in aliasing of harmonics in the signal spectrum. However, if the sampling rate is not less than the spread part of the spectrum (where most of the signal power is concentrated), that is, ~50 Hz, then the aliasing will not result in overlapping of harmonics. In this case the signal can still be recovered from its samples with minimal errors after an additional down-conversion which eliminates or substantially reduces the aliasing (this is discussed in section 4.2). This situation is shown in Figure 6b (50 Hz sampling rate). If the sampling rate is smaller than the spread part of the spectrum, then the aliasing will result in overlapping of harmonics and the signal cannot be recovered without corruption. This situation is shown in Figure 6c (25 Hz sampling rate).

4.1. Postprocessing of the RO Signal Sampled Without Aliasing

The down-converted complex signal u, sampled at a 100 Hz rate, may be directly used for the calculation of amplitude and phase, $A = [\text{Re}^2(u) + \text{Im}^2(u)]^{1/2}$; $\widetilde{\Phi} = \arctan[\text{Im}\,(u)/\text{Re}\,(u)]$. The raw phase $\widetilde{\Phi}$ is not a continuous function; that is, it contains cycle ambiguities. To calculate the continuous (or accumulated) phase Φ, the cycle ambiguities must be resolved. To achieve this, the raw signal must first be resampled at a higher rate by means of Fourier interpolation which preserves the spectrum. This reduces the phase lapse between the adjacent samples so that $|\Phi_i - \Phi_{i-1}| \ll 2\pi$. Then $\widetilde{\Phi}_i$ must be

successively compared to $\widetilde{\Phi}_{i-1}$, and 0 or $\pm 2\pi$ must be added to minimize $|\widetilde{\Phi}_i - \widetilde{\Phi}_{i-1}|$. Figure 7 shows the raw phase $\widetilde{\Phi}(t)$ and the accumulated phase $\Phi(t)$ reconstructed after resampling the RO signal from 100 to 3200 Hz.

The reconstructed phase Φ is in excess of the phase model $\Phi_{\text{mod}} = 2\pi \int f_{\text{mod}}(t)dt$ that was used for the in-real-time down-conversion of RO signal in the receiver. However, the up-converted signal with the phase $\Phi + \Phi_{\text{mod}}$ must be further corrected for the solution of the transmitter and receiver clocks and for the relativistic effects not modeled by the special GPS carrier frequency shift. Discussion of these corrections, which we introduce as $\Delta\Phi_{\text{corr}}$, is outside the scope of this paper as they have to be applied for OL and PLL tracking data alike. The technique solving for the GPS and receiver clocks is given by *Rocken and Meertens* [1991], *Melbourne et al.* [1994], *Kursinski et al.* [1997], *Zumberge et al.* [1997-1998], and *Schreiner et al.* [1998]. A detailed discussion of the special and general relativistic effects on the GPS signals is given by, for example, *Parkinson and Spilker* [1996]. After these corrections the amplitude A and the phase $\Phi + \Phi_{\text{mod}} + \Delta\Phi_{\text{corr}}$ represent the complex electromagnetic field on the LEO observation trajectory. This complex signal can be used for inversions. First, one calulates the function $\alpha(a)$, which can then be used for the reconstruction of refractivity with the Abel inversion (or for direct assimilation in NWP models). The function $\alpha(a)$ can be calculated either from phase data only under conditions of single-path propagation (above the troposphere) [*Fjeldbo et al.*, 1971; *Vorob'ev and Krasil'nikova,* 1994; *Kursinski et al.*, 1997] or from both phase and amplitude, that is, by radio holographic methods under the conditions of multipath propagation in the troposphere [*Karayel and Hinson,* 1997; *Gorbunov and Gurvich,* 1998; *Mortensen and Hoeg,* 1998; *Hocke et al.*, 1999; *Gorbunov et al.*, 2000; *Sokolovskiy,* this issue].

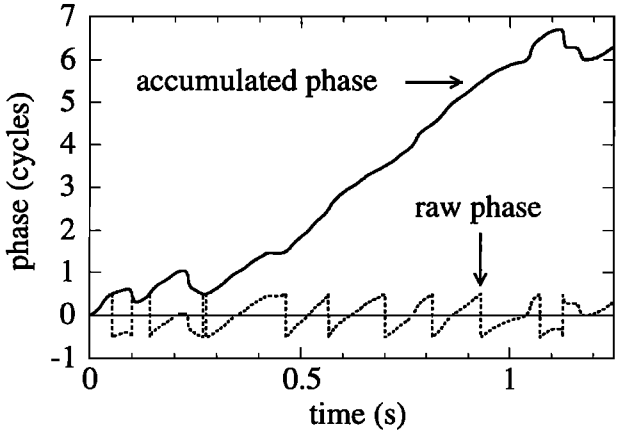

Figure 7. Reconstruction of the accumulated phase from the raw phase.

The reconstruction of the accumulated phase shown in Figure 7 assumed no noise. Noise will introduce errors in phase and amplitude (in particular, it can result in cycle slips in the reconstructed accumulated phase). To estimate the SNR in a GPS receiver for a given antenna gain, we use, as the starting point, the results published by *Melbourne et al.* [1994]. Figure 5-1 in *Melbourne et al.* [1994] shows the magnitude of thermal phase noise Δs (millimeters) for a 1 Hz sampling rate after full demodulation of the L2 signal by a replica of the P(Y) code as a function of antenna gain for some generic GPS flight receiver. For 4 and 10 dB antennas (a 4 dB antenna was used in the GPS/MET receiver, and ~10 dB gain in the direction of the Earth limb is planned in the future RO missions), $\Delta s = 0.2$ and 0.1 mm, respectively. Thus the SNR $= \lambda/2\pi\Delta s$ ($\lambda = 24.4$ cm is L2 wavelength) is 194 and 388. For an L1 C/A signal and a sampling rate different from 1 Hz the SNR differs by a factor of $\sqrt{\nu/f_{\text{samp}}}$, where $\nu = 4$ is the ratio of L1 C/A to L2 signal power, and f_{samp} is the sampling rate in hertz. For $f_{\text{samp}} = 50$ Hz the SNR = 55 and 110, and for $f_{\text{samp}} = 100$ Hz the SNR = 39 and 78. We note that these magnitudes of SNR are related to the full L1 C/A signal power that would be observed without an atmosphere. Figure 8 shows the accumulated phase reconstruction error in units of cycles without noise (Figure 8a) and with noise induced by a 4 dB antenna (Figure 8b). The errors induced by thermal noise in the retrieved refractivity are estimated in section 5.

4.2. Postprocessing of the RO Signal Sampled With Aliasing

Here we assume that the sampling rate is not less than 50 Hz, so that aliasing does not result in overlapping of harmonics (as shown in Figure 6b). The aliased spectrum is shown once again by a solid line in Figure 9. It appears that it is possible to approximately detect the shift of the center of the spectrum Δf_{shft} by calculating the maximum of cross correlation between the raw spectrum and a model of that spectrum. A rather simple model, like

$1 + \cos(2\pi f/f_{\text{samp}})$, shown in Figure 9 by a dashed line, provides feasible results. The thick-dashed vertical line marks the maximum of the cross correlation and indicates the estimated shift of the center of the spectrum Δf_{shft}. Figure 10 shows the RO signal after we down-converted it to zero mean frequency (with the use of a spline regression of the Doppler), then shifted it in the frequency domain by 20 Hz (thus simulating Doppler mismodeling), and sampled it at 50 Hz. The detected mean frequency shift of the complex signal Δf_{shft}, based on the maximum of cross correlation of the spectrum with the model function in the sliding window, is shown by the thick solid line in Figure 10. As seen, the mean frequency shift is detected fairly well. Some bias in the detected mean frequency shift below -100 km of the line-of-sight altitude can be explained by the asymmetry of the RO signal spectrum at those altitudes (see Figure 1e). In principle it is possible to use a more complicated model of the spectrum of the RO signal, which would take that asymmetry into account. The detected mean frequency shift of the RO signal as a function of time $\Delta f_{\text{shft}}(t)$ can be used as the frequency model for the additional down-conversion of the signal (which eliminates or, at least, substantially reduces aliasing) prior to the resampling and reconstructing the accumulated phase Φ and amplitude A as discussed in section 4.1. Then the phase of the RO signal is $\Phi + \Phi_{\text{mod}} + \Delta\Phi_{\text{shft}} + \Delta\Phi_{\text{corr}}$, where

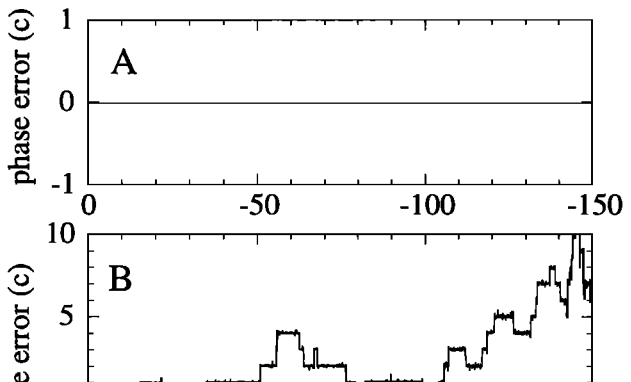

Figure 8. Phase reconstruction error after 100 Hz sampling: (a) without noise and (b) with 4 dB antenna noise.

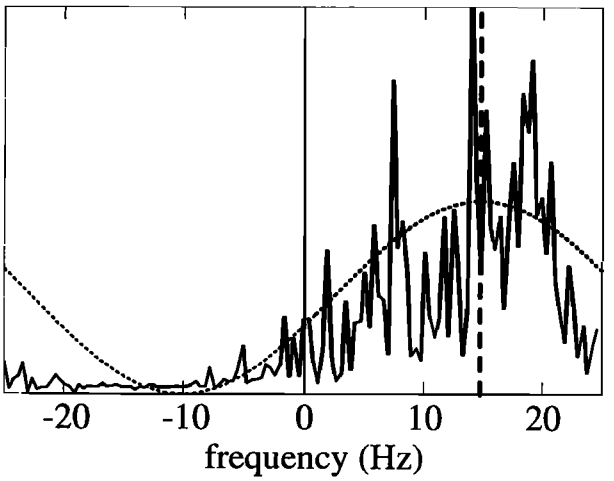

Figure 9. Estimation of the mean frequency shift of RO signal (indicated by thick vertical dashed line) by cross correlation of its spectrum (solid line) with a model (dashed line).

$\Delta\Phi_{\text{shft}} = 2\pi \int \Delta f_{\text{shft}}(t)dt$ and $\Delta\Phi_{\text{corr}}$ is the clock and relativistic correction term introduced in section 4.1. Figure 11a shows the phase reconstruction error for the RO signal with 20 Hz mean Doppler mismodeling, sampled at 50 Hz rate. As seen, the phase error is rather large. Figure 11b shows the phase reconstruction error after the additional down-conversion with the use of the $\Delta f_{\text{shft}}(t)$. As seen, the phase is reconstructed as well as in the case of 100 Hz sampling. Figure 11c shows the phase reconstruction error in the presence of thermal noise induced by a 4 dB antenna.

If the mean Doppler mismodeling is close to maximal, ± 25 Hz, and if the signal was sampled at 50 Hz rate, then it is not possible to distinguish between +25 Hz and -25 Hz frequency shift of the spectrum (i.e., there is a 50 Hz ambiguity). Thus the detection of the mean frequency shift by means of the sliding window spectral analysis must be started at high enough altitudes where Doppler mismodeling is known to be $\ll 25$ Hz and can be detected unambiguously. The detected frequency shift for each spectrum Δf^i_{shft} must be successively compared to the shift detected for the previous spectrum $\Delta f^{i-1}_{\text{shft}}$, and 0 or ± 50 Hz must be added to minimize $|f^i_{\text{shft}} - f^{i-1}_{\text{shft}}|$. The resolving of the "bandwidth ambiguities" in the frequency domain is thus similar to the resolving of the cycle ambiguities in phase domain (discussed in section 4.1).

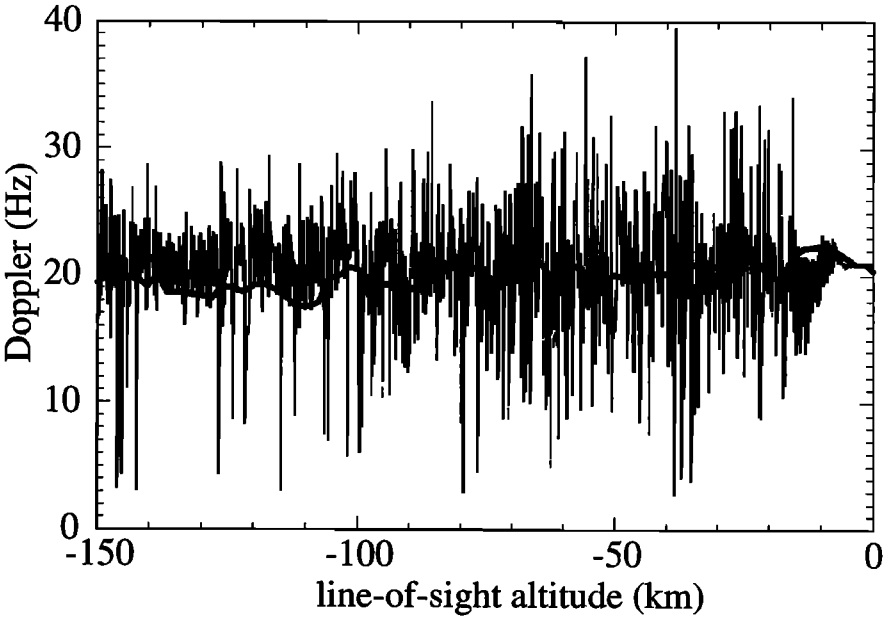

Figure 10. Estimation of the mean frequency shift of the RO signal, sampled at 50 Hz with aliasing, by the sliding window spectral analysis.

5. Example of Radio Holographic Inversion of the Sampled RO Signal

Under conditions of multipath propagation (which is the case for the modeled tropospheric RO signals), calculation of the bending angle from Doppler only (i.e., under the assumption of single-path propagation) results in large errors. Under such conditions the function $\alpha(a)$ must be calculated from the complex RO signal by radio holographic methods which take into account the multipath propagation. In this case the error of the accumulated phase (integrated Doppler) does not fully characterize the error of the bending angle and of the retrieved refractivity. The error may also depend on the radio holographic method that is used. The radio holographic methods, back propagation and radio optics, are discussed in a number of papers [*Karayel and Hinson,* 1997; *Gorbunov and Gurvich,* 1998; *Mortensen and Hoeg,* 1998; *Hocke et al.,* 1999; *Gorbunov et al.,* 2000; *Sokolovskiy,* this issue]. For the modeled "worst case" signals used in this study the back propagation method does not provide feasible results. Here we use the sliding spectral (radio optic) method which utilizes the whole spectral content of RO signal (i.e., it associates rays with all harmonics without identification and selection of local spectral maxima) introduced by *Sokolovskiy* [this issue]. The function $\alpha(a)$ calculated by this method is then subjected to the Abel inversion, and the retrieved refractivity profile is compared to the true one. Since the sliding spectral method by itself results in inversion errors in the presence of severe multipath induced by multiple superrefraction layers, the errors resulting from different sources are displayed separately.

Figure 12a shows the true radiosonde refractivity that was used for modeling of the RO signal as a thick solid line. The retrieved refractivity for which the signal was sampled at 100 Hz rate and "tracked" down to -150 km altitude of the line of sight is shown as a thin solid line. Tracking to altitudes lower than -150 km yields essentially the same inversion results. However, when tracking is stopped at higher altitudes, the inversion results can be substantially different. The dashed line shows the retrieved refractivity when tracking was stopped at -100 km, which, as seen, results in an additional negative bias in the retrieved refractivity. This indicates that the information content of the modeled worst case RO signal is important for radio holographic inversions down to about -150 km of the line-of-sight altitude. Figure 12b displays the inversion errors for both cases shown in Figure 12a.

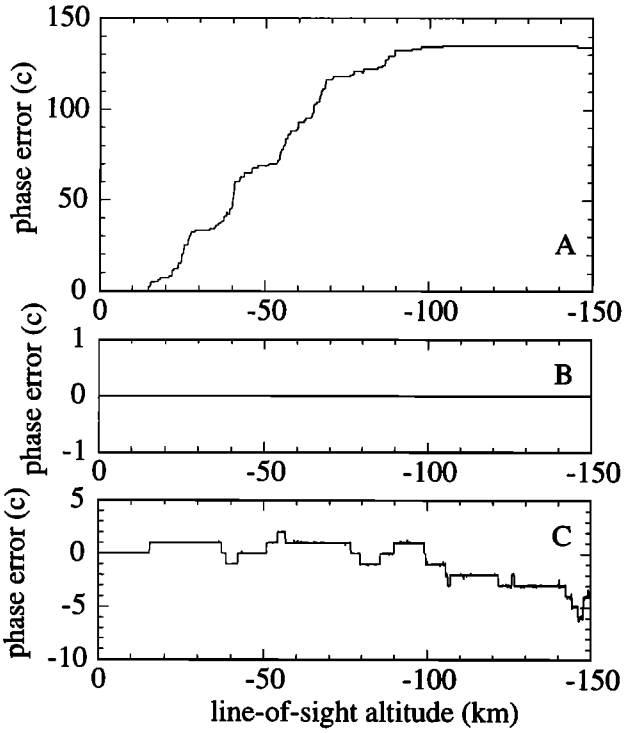

Figure 11. Phase reconstruction error after 50 Hz sampling: (a) signal with aliased spectrum, (b) after the dealiasing, and (c) with 4 dB antenna noise.

Figure 13 shows the additional inversion errors when the RO signal is tracked down to -150 km line-of-sight altitude. Figure 13a shows as dashed and solid lines the errors induced by 4 and 10 dB antenna noise for the case of 100 Hz sampling. Figure 13b shows the difference between the inversions of the signal sampled at 100 Hz and at 50 Hz rate. For both sampling rates the RO signal was down-converted to a mean frequency close to zero prior to sampling. As seen, the difference between the inversions of the 100 and 50 Hz sampled RO signals, which can be attributed to the spectral content of the signal outside the 50 Hz band (but inside the 100 Hz band), is rather small. Figure 13c shows the inversion errors introduced by aliasing in the case of 50 Hz sampling. The dashed line shows the inversion error of the RO signal with an aliased spectrum (the mean residual frequency of 20 Hz prior to 50 Hz sampling). The solid line shows the inversion error after dealiasing as discussed in section 4.2. Figure 13d shows as dashed and solid lines the errors induced by 4 and 10 dB antenna noise for 50 Hz sampling. As seen, the inversion errors due to the multipath induced by superrefraction (Figure 12b) are larger than the errors due to the antenna noise and 50 Hz sampling (Figure 13) except for the case of 50 Hz sampling with rather large aliasing (20 Hz mean Doppler mismodeling). The dealiasing reduces the inversion error to a level smaller than that induced by the antenna noise. Thus the use of 50 Hz sampling rate is feasible in the lower troposphere. The inversion errors due to the antenna noise are larger for 100 Hz than for 50 Hz sampling. The inversion method used, which associates rays with the whole spectral content of the RO signal (feasible for worst case signals) in fact is not an optimal noise filter. Thus it must be applied in the troposphere only, where the errors due to noise are still smaller than the inversion errors due to the multipath induced by superrefraction.

6. Conclusions

PLL tracking of RO signals propagated through the moist troposphere is inadequate because of the complicated structure of those signals which contain multiple tones. The multipath propagation results in a spectral bandwidth of the RO signals of ~50 Hz, strong phase and amplitude fluctuations, and large random phase accelerations. PLL tracking of such signals is sensitive to tunable parameters. In the GPS/MET mission the errors of the PLL tracking are believed to be the main source of the refractivity retrieval errors in the lower troposphere.

OL tracking of RO signals in the lower troposphere appears more feasible. It must include calculation of a Doppler model prior to an occultation. This Doppler model is based on predicted orbits and a bending angle model which is computed from refractivity climatology. A fast algorithm, appropriate for the use in the GPS receiver on board LEO, was introduced in section 2. The accuracy of the Doppler model can be about ±15-20 Hz. During an occultation the RO signal must be down-converted with the use of the Doppler model, low-pass filtered, and sampled in phase and quadrature. The estimated filter bandwidth is 100 Hz. The sampling rate need not to be larger than 100 Hz and must not be less than 50 Hz. The amplitude and the accumulated phase must be reconstructed from the sampled complex signal in postprocessing. If the sampling rate is lower than 100 Hz, an additional down-conversion must be applied to eliminate (reduce) aliasing of the signal spectrum. The frequency model for this down-conversion can be

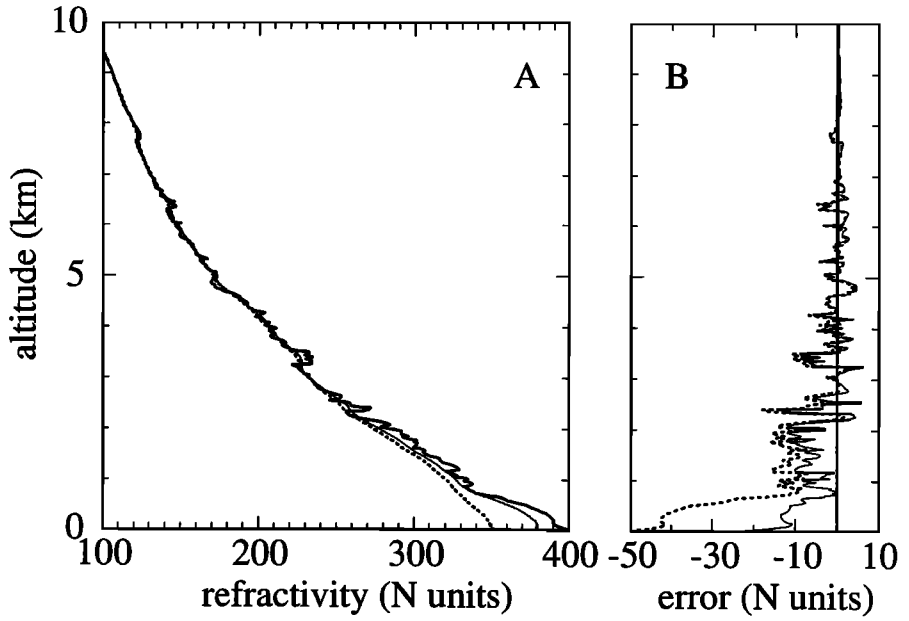

Figure 12. (a) True (radiosonde) refractivity (thick solid line); the retrieved refractivity after tracking of the RO signal down to -150 km line-of-sight altitude (thin solid line) and down to -100 km line-of-sight altitude (dashed line). (b) Refractivity retrieval errors from Figure 12a.

obtained from the sliding window spectral analysis of the signal as it was introduced in section 4.2.

Testing of the OL tracking by worst case tropospheric RO signals modeled from high-resolution topical radiosondes demonstrated stable reconstruction of the RO signal from its 50-100 Hz complex samples down to about -150 km altitude of the line of sight. Thermal noise induced by a 4-10 dB antenna results in errors of the reconstructed RO signal, which can cause up to several tens of cycle slips in the phase.

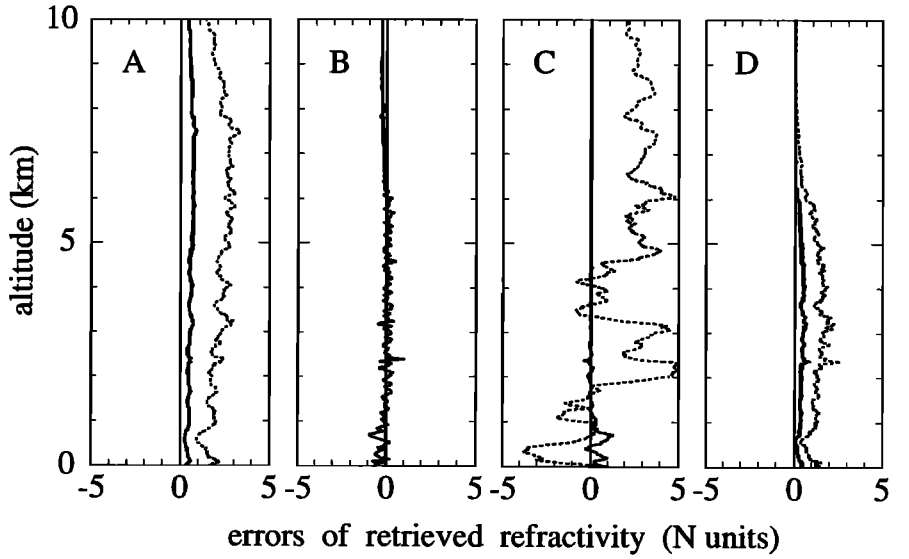

Figure 13. Refractivity retrieval errors induced by (a) thermal noise for 100 Hz sampling rate, (b) 50 Hz sampling rate as compared to 100 Hz, (c) aliasing due to 20 Hz mean frequency mismodeling and 50 Hz sampling rate, and (d) thermal noise for 50 Hz sampling rate.

The effect of the thermal noise on the reconstructed complex RO signal is translated into a refractivity retrieval error with peak magnitude up to 1-3 N units (this error may depend on the inversion technique).

All results obtained in this study assume transmission of monochromatic signals. The antenna gain necessary for demodulation of the GPS RO signals without the in-real-time extraction of phase and the use of the Doppler model for aiding demodulation under the conditions of low SNR must be evaluated in a separate study.

Acknowledgments. This work was performed as part of development of the Constellation Observing System for Meteorology Ionosphere and Climate (COSMIC) Data Analysis and Archive Center (CDAAC) at UCAR, funded by National Science Foundation (NSF) under the Cooperative Agreement ATM-9732665. I am grateful to J. Fein (NSF) for his support of the UCAR COSMIC program, to C. Rocken, W. S. Schreiner and R. J. Keeler (UCAR) for useful discussions of the subject. I am especially grateful to C. Rocken for reading the manuscript and valuable comments. I am also grateful to S. Syndegaard (University of Arizona) and to anonymous referees for their useful comments.

References

Fjeldbo, G., A.J. Kliore, and V.R. Eshleman, The neutral atmosphere of Venus as studied with the Mariner V radio occultation experiments, *Astron. J., 76*(2), 123-140, 1971.

Gorbunov, M.E., and A.S. Gurvich, Microlab-1 Experiment: Multipath effects in the lower troposphere, *J. Geophys. Res., 103*(D12), 13,819-13,826, 1998.

Gorbunov, M.E., A.S. Gurvich, and L. Kornblueh, Comparative analysis of radioholographic methods of processing of radio occultation data, *Radio Sci., 35*(4), 1025-1034, 2000.

Hocke, K., A.G. Pavelyev, O.I. Yakovlev, L. Barthes, and N. Jakowski, Radio occultation data analysis by the radio holographic method, *J. Atmos. Sol. Terr. Phys., 61*, 1169-1177, 1999.

Kaplan, E.D., *Understanding GPS, Principles and Applications,* 554 pp., Artech House, Norwood, Mass., 1996.

Karayel, E.T., and D.P. Hinson, Sub-Fresnel-scale vertical resolution in atmospheric profiles from radio occultation, *Radio Sci., 32*(2), 411-423, 1997.

Kirchengast, G., J. Hafner, and W. Poetzi, The CIRA86aQ_UoG model: An extension of the CIRA-86 monthly tables including humidity tables and a Fortran95 global moist air climatology model, *IMG/UoG Techn. Rep. 8*, Eur. Space Agency, Paris, France, 1999.

Kuo, Y.-H., C. Rocken, S. Sokolovskiy, E.R. Kursinski, D. Chu, and L. Lee, Constellation observing system for meteorology, ionosphere, and climate - COSMIC: An overview, paper presented at 4th Symposium on Integrated Observing Systems, Am. Meteorol. Soc., Long Beach, Calif., Jan. 9-14, 2000.

Kursinski, E.R., G.A. Hajj, J.T. Schofield, R.P. Linfield, and K.R. Hardy, Observing Earth's atmosphere with radio occultation measurements using the Global Positioning System, *J. Geophys. Res., 102*(D19), 23,429-23,465, 1997.

Lindal, G.F., G.E. Wood, H.B. Hotz, D.N. Sweetnam, V.R. Eshleman, and G.L. Tyler, The atmosphere of Titan: An analysis of the Voyager 1 radio occultation measurements, *Icarus, 53*, 348-363, 1983.

Lindal, G.F., J.R. Lyons, D.N. Sweetnam, V.R. Eshleman, D.P. Hinson, and G.L. Tyler, The atmosphere of Uranus: Results of radio occultation measurements with Voyager 2, *J. Geophys. Res., 92*, 14,987-15,001, 1987.

Melbourne, W.G., E.S. Davis, C.B. Dunkan, G.A. Hajj, K.R. Hardy, E.R. Kursinski, T.K. Meehan, L.E. Young, and T.P. Yunck, The application of spaceborne GPS to atmospheric limb sounding and global change monitoring, *JPL Publ., 94-18*, 147 pp., 1994.

Mortensen, D.M., and P. Hoeg, Inversion of GPS radio occultation measurements using Fresnel diffraction theory, *Geophys. Res. Lett., 25*(13), 2441-2444, 1998.

Parkinson, B.W., and J.J. Spilker, *Global Positioning System: Theory and Applications,* vol. 2, 643 pp., Am. Inst. of Aeronaut. and Astronaut., New York, 1996.

Proakis, J.G., and D.G. Manolakis, *Digital Signal Processing: Principles, Algorithms and Applications,* 969 pp., MacMillan, Old Tappan, N. J., 1992.

Rocken, C., and C. Meertens, Monitoring selective availability dither frequencies and their effect on GPS data, *Bull. Geod., 65*, 162-169, 1991.

Rocken, C., et al., Analysis and validation of GPS/MET data in the lower troposphere, *J. Geophys. Res., 102*(D25), 29,849-29,866, 1997.

Schreiner, W.S., D.C. Hunt, C. Rocken, and S. Sokolovskiy, Precise GPS data processing for the GPS/MET radio occultation mission at UCAR, in *Proceedings of the Institute of Navigation: Navigation 2000,* pp. 103-112, Alexandria, Va., 1998.

Sela, J.G., Spectral modeling at the National Meteorological Center, *Month. Weather Rev., 108*(9), 1279-1292, 1980.

Sokolovskiy, S.V., Modeling and inverting radio occultation signals in the moist troposphere, *Radio Sci.*, this issue.

Stephens, S.A., and J.B. Thomas, Controlled-root formulation for digital phase-locked loops, *IEEE Trans. Aerosp. Electron. Syst., 31*(1), 78-95, 1995.

Vorob'ev, V.V., and T.G. Krasil'nikova, Estimation of the accuracy of the atmospheric refractive index re-

covery from Doppler shift measurements at frequencies used in the NAVSTAR system, *Izv. Russ. Acad. Sci., Atmos. Oceanic Phys.*, Engl. Transl., *29*, 602-609, 1994.

Zumberge, J.F., M.M. Watkins, and F.H. Webb, Characteristics and applications of precise GPS clock solutions every 30 seconds, *Navigation, 44*(4), 449-456, 1997.

S. V. Sokolovskiy, University Corporation for Atmospheric Research, 3300 Mitchell Lane, Suite 3406, Boulder, CO 80301. (sergey@ucar.edu)

(Received December 21, 1999; revised January 29, 2001;
accepted January 30, 2001.)